Organic & Biomolecular Chemistry

Accepted Manuscript

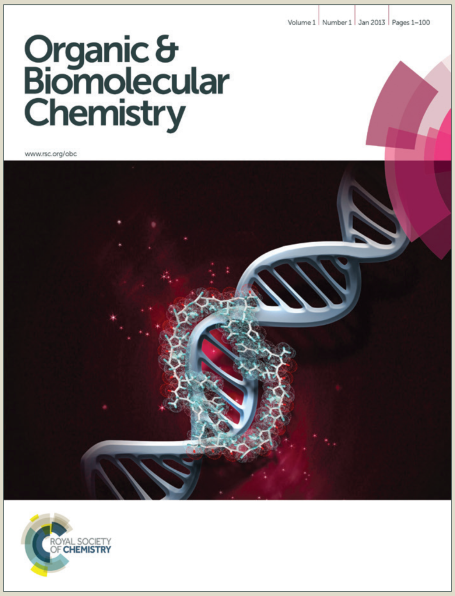

This is an *Accepted Manuscript*, which has been through the Royal Society of Chemistry peer review process and has been accepted for publication.

*Accepted Manuscripts* are published online shortly after acceptance, before technical editing, formatting and proof reading. Using this free service, authors can make their results available to the community, in citable form, before we publish the edited article. We will replace this *Accepted Manuscript* with the edited and formatted *Advance Article* as soon as it is available.

You can find more information about *Accepted Manuscripts* in the Information for Authors.

Please note that technical editing may introduce minor changes to the text and/or graphics, which may alter content. The journal's standard Terms & Conditions and the Ethical guidelines still apply. In no event shall the Royal Society of Chemistry be held responsible for any errors or omissions in this *Accepted Manuscript* or any consequences arising from the use of any information it contains.

ROYAL SOCIETY OF CHEMISTRY

www.rsc.org/obc

Cite this: DOI: 10.1039/c0xx00000x

www.rsc.org/xxxxxx

ARTICLE TYPE

# Aggregation-induced Emission Enhancement Upon $Al^{3+}$ Complexation With Tetrasulfonated Calix[4]bisazacrown Fluorescent Molecular Sensor

**Yi-Bin Ruan,[a] Alexis Depauw,[a] and Isabelle Leray*[a]**

***Received (in XXX, XXX) Xth XXXXXXXXX 20XX, Accepted Xth XXXXXXXXX 20XX***

**DOI: 10.1039/b000000x**

Aggregation-induced emission and aggregation-induced emission enhancement have attracted much attention due to its great potential in real-world applications. Up to now most of the reports are based on the restriction of the free rotation of the luminogens in the aggregates. In the present work, we found that dansyl fluorophore with typically intramolecular charge transfer characteristic also exhibited aggregation-induced emission enhancement, which was based on the change of micro-environmental polarity of the fluorophore. In the light of the phenomenon, a new water-soluble ligand bearing tetrasulfonated calix[4]arene was constructed for ratiometric detection of $Al^{3+}$ based on an aggregation-induced emission enhancement mechanism. It displayed a distinguished selectivity to $Al^{3+}$ among the tested cations in lutidine buffer solution (pH 6-7) with a detection limit of 1.8 μM. Reversible response was also demonstrated by the addition of EDTA or $F^-$.

## Introduction

Most fluorophores with planar and rigid aromatic structures, such as pyrene or perylene moieties, at high concentrations or solid state are usually weakly luminescent, which is considered to be associated with the formation of excimer/exiplex or aggregates.[1] Not until recently, aggregation-induced emission (AIE) and aggregation-induced emission enhancement (AIEE) phenomena are discovered, demonstrating that upon formation of aggregates emission efficiency is enhanced for some specific fluorophores.[2, 3] These fluorophores share a common feature that they all have a rotatable single bond, which results in non-radiative decay of excitons. While in the aggregate state, restriction of free rotation in the free ligand open up the radiative decay. Since this discovery, AIE/AIEE has been widely explored in the various fields, especially as optical sensor materials. However, it should be noted that in the aggregate state, not only the free rotation is suppressed, but also some factors like polarity are also quite different from that of the monomers in solution which sometimes may strongly influence the optical properties, especially for fluorophores with intramolecular charge transfer (ICT). This means that it's possible to envisage molecules with rigid planar structure to have AIE/AIEE effect. This can open up a new possibility to extend the structure diversity of luminogens with AIE/AIEE effect. Danysl fluorophore is an attractive signalling reporting unit for its high sensitivity to surrounding polarity.[4] Generally with increasing polarity, it shows a red shift of its emission spectrum and some specific interaction such as hydrogen bonding can lead to increase of non-radiative decay.[5] In present work, we intend to use this fluorophore to investigate polarity-induced AIE/AIEE effect.

Aluminum is the most abundant metallic element in the Earth's crust. Due to its good physical and chemical properties, it has been widely used in our daily life and thus its health concerns are considerably important. Exposure to high dose of $Al^{3+}$ can lead to neurotoxicity and deposit in bone and central nervous system.[6-8] For example, it's considered that Alzheimer's disease is highly associated with the accumulation of $Al^{3+}$ in the human body.[9] Conventional methods such as atomic absorption spectrometry and inductively coupled plasma atomic emission spectroscopy have been utilized to detect elemental aluminum and study their biological and environmental impacts. However, they usually require expensive instruments and complicated sample preparation, making them unsuitable for on-site detection. Developing low cost and real-time monitoring systems thus are highly desirable. Fluorescent chemosensors have been well developed for the detection of important analytes in biological and environmental samples.[10-12] They exhibit several advantages when compared with the conventional methods, such as the low cost, easy sample preparation, on-site detection and biological imaging applications in vivo/vitro samples. In this context, several typical binding motifs have been coupled with different chromophore/fluorophores for the detection of $Al^{3+}$, such as salicylic-schiff base,[13-17] salicylic-amino base[18-20] and triazole[21-23]. To the best of our knowledge, these approaches were carried out in solutions containing various organic solvents. And up to now still rare examples were reported for the detection of $Al^{3+}$ based on AIE mechanism. An organic ligand consisting of triphenyl pyrole was found to exhibit AIE phenomenon in the presence of $Al^{3+}$ in THF/$H_2O$ mixtures (v/v = 25/75).[24] Beside the high fraction of organic solvent, it suffered from the interference of $Pb^{2+}$ and $Zn^{2+}$. To deal with this problem, a water-soluble ligand has first to be designed and synthesized. Sulfonation is an efficient way to improve water solubility of chromophores. Furthermore, investigations on interaction of surfactant containing sulfonate with $Al^{3+}$ have shown that the strong electrostatic interaction could lead to precipitation of the complex. Their results indicated that the competition among sulfonate monomers, micelles and hydroxyl ions for Al species control the behavior of the system.[25] Therefore sulfonate group is considered as an ideal choice in our present work to deal with water solubility and binding affinity with $Al^{3+}$. For continuous work on the program of developing fluorescent chemosensors based on the framework of calix[4]arene,[26-29] we envisage to introduce the sulfonate groups on to the calix[4]arene moiety bearing dansyl as the fluorophore and investigate the interaction between sulfonate group and $Al^{3+}$ in a fluorometric manner.

## Results and discussion

The synthesis of compound **3** was accomplished according to the procedure displayed in Scheme 1, starting from the tetratosylate **1**.[30] Dansylamide was reacted with 0.5 equiv tetratosylate **1** in the presence of $K_2CO_3$ in the refluxing MeCN overnight. The crude product was isolated by column chromatography to afford **2** in 47% yield. **3** was obtained by direct sulfonation of **2** with chlorosulfonic acid, followed by neutralization with $NaHCO_3$ in pyridine/$H_2O$ mixed solution in 54% yield. **3** was well characterized by $^1H$, $^{13}C$ NMR and HRMS spectra. The 1,3-alternate conformation of **3** was deduced from the singlet peak (8H) of $ArCH_2Ar$ at 3.90 ppm in $D_2O$ (Fig. S1).

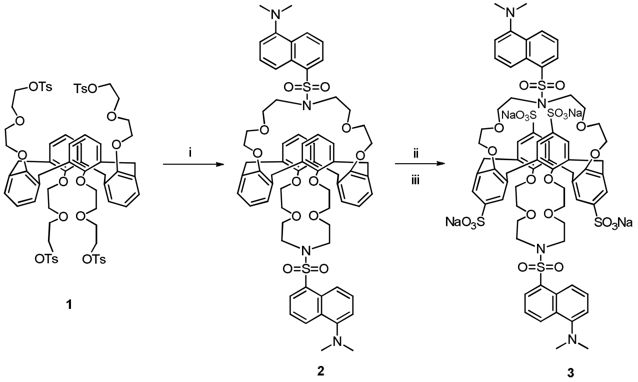

**Scheme 1.** Synthetic routine of **3**, (i) Dansylamide/$K_2CO_3$/MeCN, reflux overnight, 47%; (ii) $HSO_3Cl/CH_2Cl_2$, -10°C to RT; (iii) $H_2O$/pyridine/$NaHCO_3$, RT, 54%.

Photophysical behavior of **2** was investigated in EtOH-$H_2O$ mixed solution with different volumetric fractions of $H_2O$, as shown in Fig.1. It's quite surprising to find that **2** exhibits an AIEE effect in EtOH/$H_2O$ mixed solution. With increasing water fraction to 40%, progressive fluorescence quenching with a red shift from 532 nm to 550 nm is observed. This is usually explained by the increase of solvent polarity by increasing water fraction, which can stabilize the charge separated state in the excited state and consequently lead to the red shift of the fluorescence spectra. In contrast, when the fraction of $H_2O$ exceeds 40%, then a level-off tail absorption band is observed and correspondingly emission spectra display remarkable blue shift from 550 to 500 nm and fluorescence enhancement (about 2.7 folds when water fraction is 0.6 compared with 0.4). This is in contrast to our expectation that increasing polarity would induce the red shift of the ICT band. As we know that **2** is not soluble in $H_2O$, thus increasing water fraction could lead to the formation of aggregate or small particles, which can be deduced from the level-off tail absorption. Fluorescence quenching is generally observed during the aggregation mainly because of the formation of H-aggregate. However, it is quite different in our case. This can be attributed to dramatically reduced micro-environmental polarity of dansyl fluorophore in the aggregated state which may increase the radiative efficiency and meanwhile the bulk steric effect caused by calix[4]arene moiety prevented the compact stacking between the dansyl fluorophores. When the water fraction exceeds 60%, fluorescence intensity is slightly quenched without wavelength shift, indicating that precipitation of ligands from the solution starts occurring. It's therefore here we can conclude that formation of stable aggregates of **2** in $H_2O$ can increase the fluorescence efficiency. This phenomenon can be utilized as a new fluorescent sensing approach based on analyte-induced formation of aggregates or small particles to construct a less polar micro-environment for ICT type fluorophores.

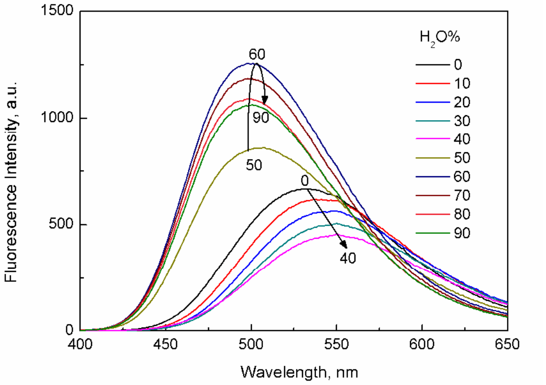

**Fig.1** Fluorescence spectra of **2** in EtOH-$H_2O$ mixed solution with different volumetric fractions of $H_2O$; [**2**] = 10 μM, $\lambda_{ex}$ = 338 nm.

The pH-dependent absorption and emission spectra of **3** were recorded in $H_2O$. As shown in Fig. S3, it exhibits a broad absorption band centered at 328 nm and an emission band at 579 nm under neutral and basic condition, which can be attributed to intramolecular charge transfer from dimethylamino group to sulfonyl group. By decreasing pH of the solution with the addition of $HClO_4$, absorption band at 328 nm decreases and new peaks at 320 and 285 nm appear, which is characteristic of dansyl fluorophore when its dimethylamino group is protonated. Meanwhile, gradual decrease of the fluorescence intensity at 579 nm was observed. This can be attributed to the fact that protonation of the dimethylamino group blocks the intramolecular charge transfer. The $pK_a$ of **3** in $H_2O$ was obtained by fitting from the titration to be 4.7. At pH 6 (in lutidine buffer) **3** is weakly fluorescent with a quantum yield $\Phi_F$ of 3.8%, mainly because of high polarity and hydrogen bonding interaction between $H_2O$ and dansyl fluorophore rather than protonation of dimethylamino group. Spectral response of **3** to $Al^{3+}$ was then examined in lutidine buffer solution at pH 6.0. Fig. 2 displays evolution of the emission spectra of **3** upon $Al^{3+}$ addition. When the concentration of $Al^{3+}$ is lower than 0.1 mM, there is a gradual fluorescence enhancement and emission band blue shift from 576 nm to 530 nm. It reaches a plateau when the concentration is over 0.1 mM. Due to a 46 nm blue shift, it's possible for us to detect $Al^{3+}$ in a ratiometric method. Ratio of fluorescence intensity at 540 and 640 nm as the functions of concentrations of added $Al^{3+}$ is plotted, as shown in Fig. 1 (inset). A nice linear dependence is obtained ranging from 0 to 0.1 mM. According to the 3σ/k, the detection limit of our protocol was calculated to be 1.8 μM, meeting with the requirement of WHO with a limit of 7.41 μM $Al^{3+}$ in drinking water.[31] Beside this, kinetics profile between **3** and $Al^{3+}$ shows that fluorescence intensity was enhanced immediately after addition of $Al^{3+}$ without waiting time (Fig. 3). The reversibility between **3** and $Al^{3+}$ was investigated in lutidine buffer solution at pH 6.0, as illustrated in Fig. S4. With the addition of 2 equiv of NaF or $Na_2$EDTA with respect to $Al^{3+}$, fluorescence spectra of **3** was recovered and nearly overlapped with free ligand. During the titration with $Al^{3+}$ (Fig. 4), the absorption band of **3** at 328 nm shows a little red shift to 335 nm, which is quite close to that of **2** with neutral charge, probably indicating that partial negative charges were neutralized by $Al^{3+}$. Meanwhile, level-off tail absorption band ranging in long wavelength region (450-500 nm) increases due to scattering effect from the gradual formation of aggregates/particles in the solution. It should be noted that the scattering effect usually lead to a fluctuation of fluorescence intensity, which may result in poor stability of the sensing approaches. Fortunately, here we can detect $Al^{3+}$ in a ratiometric manner that can greatly remove this adverse effect.

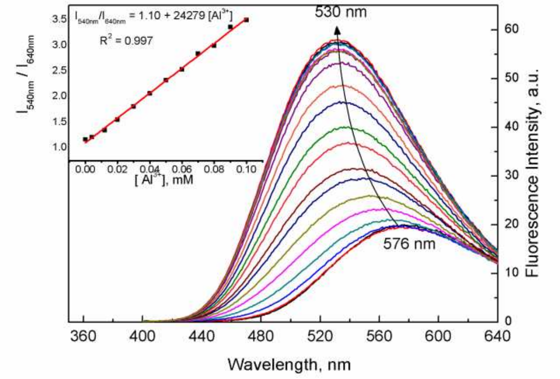

**Fig. 2** Fluorescence spectra of **3** in the presence of increasing concentrations of $Al^{3+}$ in lutidine buffer solution (pH = 6.0, 10 mM); inset: plot of ratiometric response $I_{540}/I_{640}$ against $Al^{3+}$ concentrations; [**3**] = 10 μM, $\lambda_{ex}$ = 330 nm.

In order to get insight into sensing mechanism of our protocol, we first investigated pH effect on the binding ability of **3** to $Al^{3+}$. As mentioned above, dansylamide fluorophore is sensitive to pH change. Protonation on dimethylamino group inhibits intramolecular charge transfer and decreases its emission intensity. However, no wavelength shift for ICT band is observed in the tested pH range (4-9) and thus ratio of fluorescence intensity at 540 nm and 640 nm keeps constant under different pH conditions, as shown in Fig. 5. While in the presence of $Al^{3+}$, the ratio of resultant complex shows a maximum at pH 6 and decreases dramatically when pH deviates 6 (Fig. 5). When pH is lower than 5 or higher than 8, the addition of $Al^{3+}$ almost shows no influence on the ratio value. It's well known that the existing forms of aluminum depend closely on pH, as shown in Fig. 5 (top).[32] In pure water, when the pH is lower than 4, more than 90% of aluminum exists as the free $[Al(H_2O)_6]^{3+}$; with increase of pH but lower than 7, aluminum hydrolyzes to produce precipitate $Al(OH)_3$; and when the pH is higher than 7, $Al(OH)_3$ is again transferred into $Al(OH)_4^-$. The pH effect on the spectral response of **3** to $Al^{3+}$ is quite similar to the curve of fraction distribution of $Al(OH)_3$ in water under different pH conditions, though with a narrower half-peak width. It's supposed that **3** with four negative charge can be adsorbed through electrostatic interaction onto the $Al(OH)_3$ colloid surface covered with positive charge. The electrostatic interaction was verified by the reference compound **2**. Under the identical condition in EtOH/Lutidine buffer (9:1, pH 6.0) (Fig. 6), blue shift and fluorescence enhancement are observed for **3** while they do not occur on **2**.

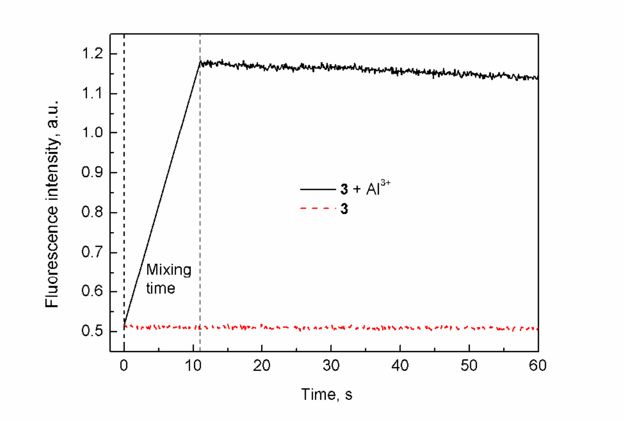

**Fig. 3** Kinetic profile of **3** in the presence of $Al^{3+}$ in lutidine buffer solution (pH = 6.0, 10 mM), fluorescence intensity was recorded at 540 nm; [**3**] = 10 μM, [$Al^{3+}$] = 25 μM, $\lambda_{ex}$ = 328 nm.

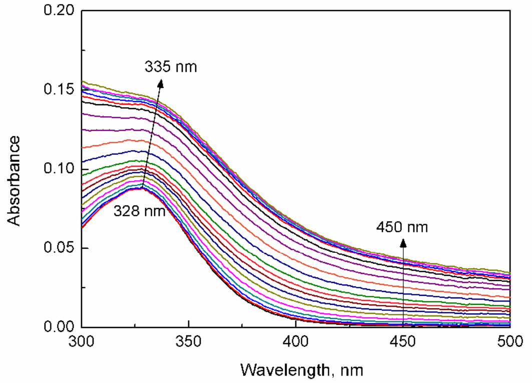

**Fig. 4** Absorption of **3** in the presence of increasing concentrations of $Al^{3+}$ in lutidine buffer solution (pH = 6.0, 10 mM); [**3**] = 10 μM.

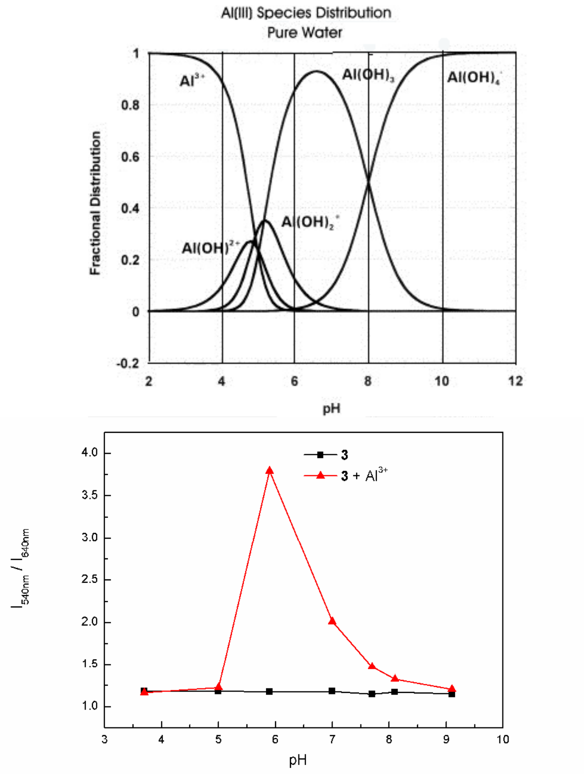

**Fig. 5** (Top) Al(III) species distribution as a function of pH in pure water, cited from the reference;[32] (bottom) the pH effect on the change of fluorescence intensity at 533 nm of **3** before and after addition of $Al^{3+}$ in lutidine solution (10 mM), $\lambda_{ex}$ = 328 nm; [**3**] = 10 µM and the pH effect of species of $Al^{3+}$ in pure water.

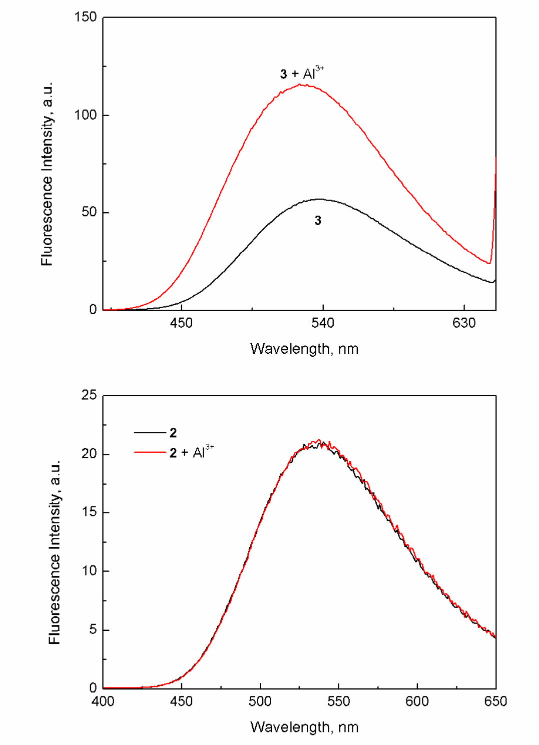

**Fig. 6** Fluorescence spectra of **3** (top) and **2** (bottom) in the absence and presence of $Al^{3+}$ in EtOH and lutidine buffer solution (pH = 6.0, 10 mM) mixed solution ($v_{EtOH}$:$v_{Lutidine}$ = 9:1); [**2**] = [**3**] = 10 µM, [$Al^{3+}$] = 0.1 mM, $\lambda_{ex}$ = 328 nm for **3**and , $\lambda_{ex}$ = 338 nm for **2**.

Fluorescence anisotropy measurement is a powerful approach to study the aggregation phenomenon. As can be seen from Fig. 7, free ligand **3** shows very small anisotropy with the average value at 0.05, which is due to the rapid rotation of fluorophore in its lifetime scale. It's quite surprising to find that with the addition of 10 equiv of $Al^{3+}$, anisotropy value of the resultant complex was increased to 0.23, as shown in Fig. 7. The significant increase of the anisotropy strongly demonstrates that free ligand **3** is adsorbed onto large particles which results in decrease of the rotational diffusion rate. Decrease of the micro-environmental polarity of ICT characteristic dansyl fluorophore in the aggregates results in the fluorescence enhancement and blue shift. Dynamic light scattering (DLS) was also carried out to confirm the aggregation process. As illustrated by Fig. 8, the polydisperse distribution of particles ranging from hundreds nm to µm is consistent with our assumption of formation of aggregate between $Al(OH)_3$ and ligand **3** under this condition. Herein we propose the sensing mechanism for our protocol, as presented in Scheme 2. Under the pH 6, formation of $Al(OH)_3$ with positive charge can adsorb negative-charged **3** to form an aggregate. A reduce of micro-environmental polarity of ICT characteristic dansyl fluorophore results in the fluorescence enhancement and blue shift. And the bulk steric effect resulted from calix[4]arene moiety prevents formation of compact H-aggregates and retains the high fluorescence quantum yield. These two factors together contribute the blue shift and fluorescence enhancement.

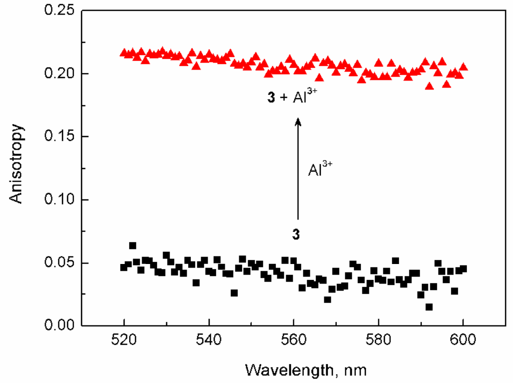

**Fig. 7** Anisotropy of **3** in the absence and presence of $Al^{3+}$ in lutidine buffer solution (pH = 6.0, 10 mM); [**3**] = 10 µM, [$Al^{3+}$] = 0.1 mM, $\lambda_{ex}$ = 328 nm.

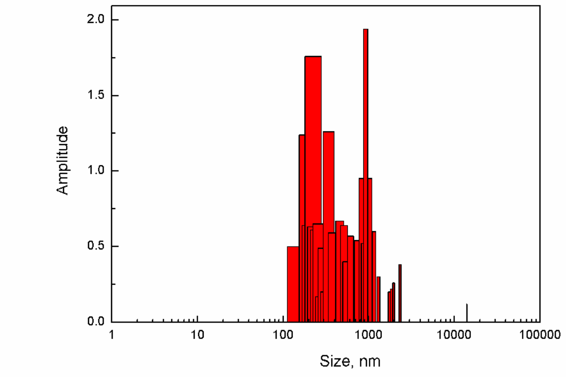

**Fig. 8** Dynamic light scattering of **3** in the presence of $Al^{3+}$ in lutidine buffer solution (pH = 6.0, 10 mM); [3] = 10 µM, [$Al^{3+}$] = 0.12 mM.

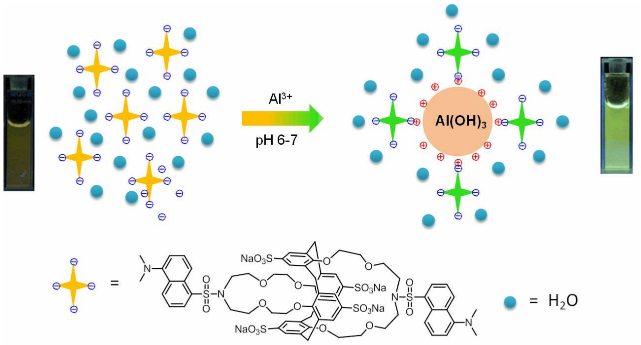

**Scheme 2.** Schematic illustration of interaction between **3** and $Al^{3+}$.

Selectivity of **3** to $Al^{3+}$ over a wide range of metal ions was then screened in lutidine buffer solution at pH 6.0. As shown in Fig. 9, the addition of very high concentrations of alkali metals $Na^+$, $K^+$, $Li^+$, alkaline earth metal $Mg^{2+}$, $Ca^{2+}$, $Ba^{2+}$ at 10 mM level and transition metal ions $Eu^{3+}$, $La^{3+}$, $Cd^{2+}$, $Co^{2+}$, $Cu^{2+}$, $Fe^{2+}$, $Hg^{2+}$, $Mn^{2+}$, $Ni^{2+}$, $Pb^{2+}$ and $Zn^{2+}$ at 0.1 mM show almost no effect on the spectral properties of **3**. The addition of $Fe^{3+}$ (0.1 mM), however, decreases the fluorescence intensity without wavelength shift. In contrast, only the addition of $Al^{3+}$ (0.1 mM) induces remarkable fluorescence enhancement concomitant with large blue shift from 576 to 530 nm and fluorescence color change from dark yellow to bright green. Considering the large blue shift of the wavelength with respect to $Al^{3+}$, selectivity is expressed as the ratio of fluorescence intensity at 540 nm and 640 nm, as shown in Fig. 11. It demonstrates that **3** shows very high selectivity to $Al^{3+}$ over other metal ions. Competition experiment of **3** to $Al^{3+}$ in the presence of other competing metal ions was also carried out. As shown in Fig. 10, all the tested competing ions except $Cu^{2+}$ and $Fe^{3+}$ hardly produced interference on the detection of $Al^{3+}$. The presence of $Cu^{2+}$ and $Fe^{3+}$ induced fluorescence quenching to different extents; however, they all showed large blue shift compared with free ligand **3**. When the ratio of fluorescence intensity at 540 nm and 640 nm was used to establish the competition experiment, the interference of $Cu^{2+}$ was eliminated and $Fe^{3+}$ was reduced, as shown in Fig. 11. Therefore **3** was demonstrated to be a promising selective fluorescent chemosensor for aluminum in complex samples.

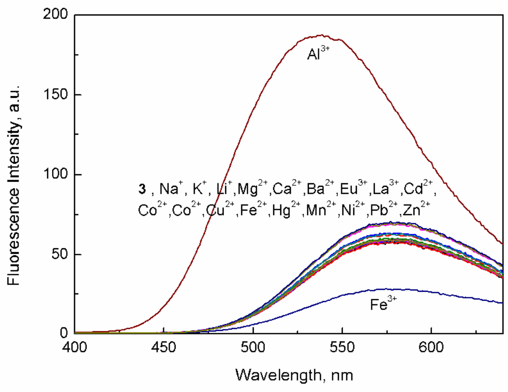

**Fig. 9** Absorption and fluorescence spectra of **3** in the presence of various metal ions in lutidine buffer solution (pH = 6.0, 10 mM); [**3**] = 10 μM, alkali and alkaline earth metal ions were 10 mM, and the others were 0.1 mM, $\lambda_{ex}$ = 328 nm.

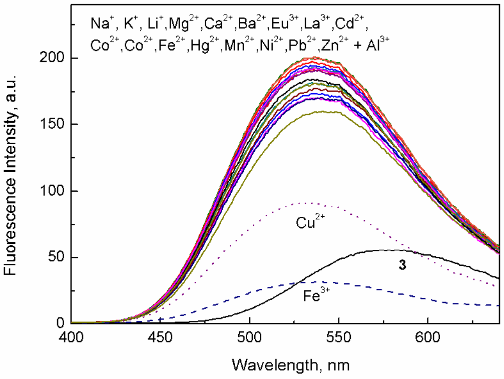

**Fig. 10** Fluorescence spectra of **3** in the coexistence of various metal ions and $Al^{3+}$ in lutidine buffer solution (pH = 6.0, 10 mM); [**3**] = 10 μM, alkali and alkaline earth metal ions were 10 mM, and the others were 0.1 mM, $\lambda_{ex}$ = 328 nm.

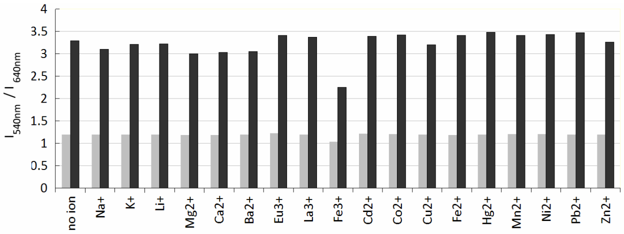

**Fig. 11** Ratiometric response $I_{540}/I_{640}$ of **3** in the presence of selected metal ions in lutidine buffer solution (pH = 6.0, 10 mM). The light bars represent the response of **3** in the presence of selected cations; the dense bars represent the response upon an addition of $Al^{3+}$ to a solution of **3** in the presence of selected cations; [**3**] = 10 μM, alkali and alkaline earth metal ions were 10 mM, and the others were 0.1 mM, $\lambda_{ex}$ = 328 nm.

## Conclusions

In conclusion, the new water-soluble fluorescent chemosensor **3** exhibits very high selectivity to $Al^{3+}$ under weak acid condition pH 6.0. Remarkable fluorescence blue shift and about 3-fold enhancement were observed due to the aggregation of **3** on colloid particles of $Al(OH)_3$, which was verified by the increase of absorption tail band, pH effect, DLS, anisotropy measurement and also a reference compound **2**. The change of the micro-environmental polarity of ICT characteristic dansyl fluorophore resulted in the fluorescence enhancement and blue shift. The selectivity of our protocol stems from the unique character of the formation of positive-charged $Al(OH)_3$ colloid particles around pH 6.0 and its strong binding affinity with sulfonate. Thus the vast choices of the sulfonated chromophore/fluorophores with different ICT characteristics may easily extend our strategy for the selective detection of $Al^{3+}$.

## Experimental section

### Materials and methods

Absorption spectra were recorded on a Cary5000 spectrophotometer and corrected emission spectra were performed on Jobin-Yvon Spex Fluorolog 1681 or FluoroMax4 spectrofluorometers (1 cm quartz cell was used). Stock solution (1.0 mM) of compound **3** was prepared in $H_2O$. Stock solutions of metal nitrate/perchlorate salts were prepared in $H_2O$, respectively.

The tested metal salts included $Al(NO_3)_3{\cdot}9H_2O$, NaSCN, KSCN, $LiClO_4$, $Mg(ClO_4)_2$, $Ca(ClO_4)_2{\cdot}4H_2O$, $Ba(ClO_4)_2$, $FeCl_3{\cdot}6H_2O$, $Eu(NO_3)_3{\cdot}6H_2O$, $La(NO_3)_3{\cdot}4H_2O$, $Cd(ClO_4)_2{\cdot}H_2O$, $Co(ClO_4)_2{\cdot}6H_2O$, $Cu(ClO_4)_2{\cdot}6H_2O$, $Fe(ClO_4)_2{\cdot}xH_2O$, $Hg(ClO_4)_2{\cdot}6H_2O$ $Mn(ClO_4)_2{\cdot}6H_2O$, $Ni(ClO_4)_2{\cdot}6H_2O$, $Pb(ClO_4)_2{\cdot}H_2O$, and $Zn(ClO_4)_2{\cdot}6H_2O$.

### Synthesis of ligands

**2**: Dansylamide (0.114 g, 0.46 mmol) and $K_2CO_3$ (0.16 g, 1.15 mmol) in dry MeCN (20 mL) was stirred at room temperature for 30 min followed by the addition of compound **1** (0.32 g, 0.23 mmol in MeCN (10 mL) ) at one port. The resulting mixture was refluxed overnight. Then solvent was evaporated and the residual was dissolved in $CHCl_3$, washed with $H_2O$ twice. The organic layer was dried over $MgSO_4$ and evaporated to obtain crude product. It was purified by column chromatograph over silica (elute: DCM/MeOH (99:1)) to obtain pure product (0.25 g, 47%). $^1H$ NMR (400 MHz, $CDCl_3$): δ 8.54 (d, $J$ = 8.2 Hz, 2H), 8.33 (d, $J$ = 8.7 Hz, 2H), 8.18 (dd, $J$ = 7.3, 1.4 Hz, 2H), 7.59 (t, $J$ = 7.8 Hz, 2H), 7.53 (t, $J$ = 7.4 Hz, 2H), 7.20 (d, $J$ = 7.8 Hz, 2H), 7.04 (d, $J$ = 7.3 Hz, 8H), 6.79 (t, $J$ = 7.4 Hz, 4H), 3.82 (s, 8H), 3.47 (m, 16H), 3.40 (t, $J$ = 5.0 Hz, 8H), 3.04 (t, $J$ = 5.0 Hz, 8H), 2.89 (s, 12H); $^{13}C$ NMR (100 MHz, $CDCl_3$): 157.3, 151.8, 135.3, 133.6, 130.3, 130.2, 130.1, 129.7, 129.3, 128.1, 123.2, 122.5, 119.7, 115.3, 70.8, 70.3, 69.5, 47.5, 45.5, 38.2 ppm; HRMS (ESI) $m/z$ calcd for $C_{68}H_{76}N_4NaO_{12}S_2$ [M + $Na^+$] 1227.4799, found 1227.4822.

**3:** To a solution of compound **2** (110 mg, 0.091 mmol) in dry DCM (3 mL) was added $HSO_3Cl$ (120 µL in 3 mL DCM) dropwise at -20°C. After stirring at room temperature for 3h, the solution was poured into ice-water solution and adjusted pH to 7 with $NaHCO_3$. The aqueous solution was evaporated to dry and redissolved in pyridine (6 mL) and water (2 mL). After stirring at room temperature for 2 h, the solution was concentrated (about 1.0 mL). Large precipitate was obtained by the addition of addition of acetone. The precipitate was again dispersed in 0.5 mL $H_2O$ at 30°C. The insoluble residual was filtered off and washed with acetone to obtain the pure product (80 mg, 54%). $^1H$ NMR (400 MHz, $D_2O$): δ 8.34 (d, $J$ = 8.7 Hz, 2H), 8.10 (d, $J$ = 7.4 Hz, 2H), 8.06 (d, $J$ = 8.7 Hz, 2H), 7.63 (t, $J$ = 8.2 Hz, 2H), 7.58 (t, $J$ = 7.8 Hz, 2H), 7.43 (s, 8H), 7.28 (d, $J$ = 7.8 Hz, 2H), 3.90 (s, 8H), 3.39 (m, 16H), 3.14 (t, $J$ = 5.0 Hz, 8H), 2.81 (t, $J$ = 5.0 Hz, 8H), 2.73 (s, 12H); $^{13}C$ NMR (100 MHz, $CDCl_3$): 159.2, 150.4, 137.5, 133.8, 130.0, 129.4, 129.1, 128.9, 126.6, 124.2, 123.2, 119.8, 116.1, 70.0, 68.6, 46.4, 45.0, 36.9 ppm; HRMS (ESI) $m/z$ calcd for $C_{68}H_{72}N_4Na_3O_{24}S_6$ [M - $Na^+$] 1589.2554, found 1589.2628.

## Notes and references

[a] *PPSM,(UMR8531) Institut d'Alembert, ENS Cachan, CNRS, 61 av President Wilson, F-94230 Cachan, France;*
*E-mail: Isabelle.LERAY@ppsm.ens-cachan.fr*

† Electronic Supplementary Information (ESI) available: [Some related spectroscopic data and NMR spectra of Ligand **2** and **3**]. See DOI: 10.1039/b000000x/

1. S. A. Jenekhe and J. A. Osaheni, *Science*, 1994, **265**, 765-768.
2. Y. Hong, J. W. Lam and B. Z. Tang, *Chem Commun*, 2009, 4332-4353.
3. Y. Hong, J. W. Lam and B. Z. Tang, *Chem. Soc. Rev.*, 2011, **40**, 5361-5388.
4. Ü. Ocak, M. Ocak and R. A. Bartsch, *Inorg. Chim. Acta*, 2012, **381**, 44-57.
5. T. Sanjoy Singh and S. Mitra, *J. Lumin.*, 2007, **127**, 508-514.
6. M. Kawahara, K. Muramoto, K. Kobayashi, H. Mori and Y. Kuroda, *Biochem. Biophys. Res. Commun.*, 1994, **198**, 531-535.
7. S. R. Paik, J. H. Lee, D. H. Kim, C. S. Chang and J. Kim, *Arch. Biochem. Biophys.*, 1997, **344**, 325-334.
8. P. F. Good, C. W. Olanow and D. P. Perl, *Brain Research*, 1992, **593**, 343-346.
9. V. B. Gupta, S. Anitha, M. L. Hegde, L. Zecca, R. M. Garruto, R. Ravid, S. K. Shankar, R. Stein, P. Shanmugavelu and K. S. Jagannatha Rao, *Cell Mol. Life Sci.*, 2005, **62**, 143-158.
10. B. Valeur and I. Leray, *Coord. Chem. Rev.*, 2000, **205**, 3-40.
11. A. P. de Silva, H. Q. N. Gunaratne, T. Gunnlaugsson, A. J. M. Huxley, C. P. McCoy, J. T. Rademacher and T. E. Rice, *Chem. Rev.*, 1997, **97**, 1515-1566.
12. I. Leray and B. Valeur, *Eur. J. Inorg. Chem.*, 2009, 3525-3535.
13. S. Kim, J. Y. Noh, K. Y. Kim, J. H. Kim, H. K. Kang, S. W. Nam, S. H. Kim, S. Park, C. Kim and J. Kim, *Inorg. Chem.*, 2012, **51**, 3597-3602.
14. K. K. Upadhyay and A. Kumar, *Org. Biomol.Chem.*, 2010, **8**, 4892-4897.
15. D. Maity and T. Govindaraju, *Eur. J. Inorg. Chem.*, 2011, 5479-5485.
16. A. Sahana, A. Banerjee, S. Das, S. Lohar, D. Karak, B. Sarkar, S. K. Mukhopadhyay, A. K. Mukherjee and D. Das, *Org. Biomol.Chem.*, 2011, **9**, 5523-5529.
17. M. Arduini, F. Felluga, F. Mancin, P. Rossi, P. Tecilla, U. Tonellato and N. Valentinuzzib, *Chem. Commun.*, 2003, 1606-1607.
18. T. H. Ma, M. Dong, Y. M. Dong, Y. W. Wang and Y. Peng, *Chem. Eur. J.*, 2010, **16**, 10313-10318.
19. M. Dong, Y. M. Dong, T. H. Ma, Y. W. Wang and Y. Peng, *Inorg. Chim. Acta*, 2012, **381**, 137-142.
20. Y. Lu, S. S. Huang, Y. Y. Liu, S. He, L. C. Zhao and X. S. Zeng, *Org. Lett.*, 2011, **13**, 5274-5277.
21. S. H. Kim, H. S. Choi, J. Kim, S. J. Lee, D. T. Quang and J. S. Kim, *Org. Lett.*, 2010, **12**, 560-563.
22. D. Maity and T. Govindaraju, *Chem. Commun.*, 2010, **46**, 4499-4501.
23. D. Maity and T. Govindaraju, *Chem. Commun.*, 2012, **48**, 1039-1041.
24. T. Y. Han, X. Feng, B. Tong, J. B. Shi, L. Chen, J. G. Zhi and Y. P. Dong, *Chem. Commun.*, 2012, **48**, 416-418.
25. P. Somasundaran, K. P. Ananthapadmanabhan and M. S. Celik, *Langmuir*, 1988, **4**, 1061-1063.
26. I. Leray, Z. Asfari, J. Vicens and B. Valeur, *J. Chem. Soc., Perkin Trans. 2*, 2002, 1429-1434.
27. R. Metivier, I. Leray and B. Valeur, *Photochem. Photobio. Sci.*, 2004, **3**, 374-380.
28. J. P. Malval, I. Leray and B. Valeur, *New J. Chem.*, 2005, **29**, 1089-1094.
29. V. Souchon, I. Leray and B. Valeur, *Chem. Commun.*, 2006, 4224-4226.

30. S. K. Kim, W. Sim, J. Vicens and J. S. Kim, *Tetrahedron Lett.*, 2003, **44**, 805-809.
31. W. W. H. O. Geneva, *Guidelines for drinking water quality 4th edition*, 2011.
32. K. M. Elkins and D. J. Nelson, *Coord. Chem. Rev.*, 2002, **228**, 205-225.